ISSN 1070-3632, Russian Journal of General Chemistry, 2015, Vol. 85, No. 1, pp. 116–122. © Pleiades Publishing, Ltd., 2015.
Original Russian Text © E.A. Katlenok, A.A. Zolotarev, K.P. Balashev, 2015, published in Zhurnal Obshchei Khimii, 2015, Vol. 85, No. 1, pp. 124–131.

Structure, Optical, and Electrochemical Properties of Pd(II), Pt(II), Rh(III), and Ir(III) Complexes with Metallated 2-Phenylbenzothiazole and Chelating 2-(1,3-Benzothiazol-2-yl)phenol

E. A. Katlenok[a], A. A. Zolotarev[b], and K. P. Balashev[a]

[a] *Herzen Russian State Pedagogical University, nab. r. Moiki 48, St. Petersburg, 191186 Russia*
e-mail: balashevk@mail.ru

[b] *St. Petersburg State University, St. Petersburg, Russia*

Received July 15, 2014

Abstract—Structures of *cis*-C,C-[M(bt)$_2$hbt] [M = Rh(III) or Ir(III)] and *trans*-N,N-[M(bt)hbt] [M = Pd(II) or Pt(II)] complexes with C,N-metallated 2-phenylbenzothiazole and N,O-chelating 2-(1,3-benzothiazol-2-yl)-phenol in crystalline form as well as in $CDCl_3$ solution have been elucidated by means of X-ray diffraction analysis and ^{1}H and ^{13}C NMR spectroscopy.

Keywords: cyclometallated complex, rhodium, iridium, platinum, palladium, molecular structure, optical properties, electrochemical properties

DOI: 10.1134/S107036321501020X

Cyclometallated complexes of platinum group metals are of special interest [1, 2] due to their room temperature phosphorescence properties and reversibility of electrochemical transfer of outer-sphere electron enabling their widespread application in organic light-emitting diodes [3], photocatalysts [4], luminescent labels for biological systems [5], and chemosensors [6]. Benzothiazole metallated chelating ligands containing two sulfur atoms are capable of donor-acceptor interaction with additional metal cation making the compounds in question promising for heavy metals sensors applications [7].

Here we report on the study of structure as well as optical and electrochemical properties of [M(bt)$_2$(hbt)] [M = Rh(III) (**I**) or Ir(III) (**II**)] and [M(bt)hbt] [M = Pd(II) (**III**) or Pt(II) (**IV**)] complexes in comparison with [M(bt)$_2$En]PF_6 and [M(bt)En]PF_6 complexes (bt$^-$ and hbt$^-$ stand for deprotonated forms of 2-phenylbenzothiazole and 2-(1,3-benzothiazol-2-yl)phenol, respectively; En is ethylenediamine) (Scheme 1).

According to X-ray diffraction analysis (Fig. 1), the [M(bt)$_2$hbt] complexes exist in the form of *cis*-C,C isomers. The substitution of Ir(III) with Rh(III) (Table 1) had practically no influence on the bond lengths between the metal and the ligand donor atoms N(bt$^-$), C(bt$^-$), and O(hbt$^-$) but was accompanied with elongation of the Rh(III)–N(hbt$^-$) bond by 0.03 Å. Bond angles of donor atoms of the ligands in the complexes of Rh(III) and Ir(III) differed by less than 1.2°. The deviation of the *trans*-located N(bt) donor atoms from the plane by ≈8° led to a distortion of octahedral positioning of the ligands donor atoms around Rh(III) and Ir(III). Phenyl and benzothiazole components of the six-membered chelate {M(hbt)}

Scheme 1.

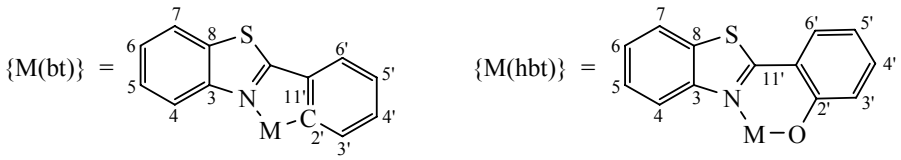

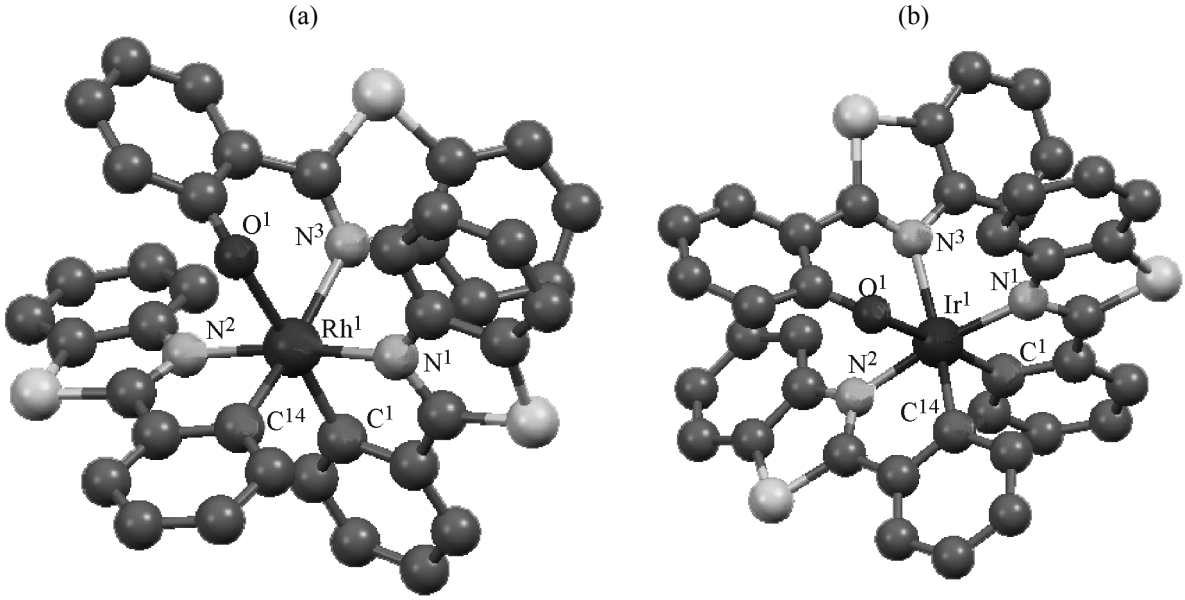

Fig. 1. Spatial structure of the $[Rh(bt)_2hbt]$ (a) and $[Ir(bt)_2hbt]$ (b) complexes in the crystal state (H atoms are omitted).

deviated from the plane formed by the metal atoms, oxygen, and nitrogen by ≈40° and ≈17°, respectively.

Isomeric *cis*-C,C structure of the $[M(bt)_2hbt]$ complexes was preserved in the $CDCl_3$ solution. That was confirmed by non-equivalence of signals of hydrogen and carbon atoms of the two metallated ligands $\{M(bt)_2\}$ in the complexes (Table 2) as well as by mutual anisotropic action of circular currents of their phenyl groups leading to the upfield shift of $H^{3'}$ signals by 1.3–1.0 ppm as compared to those of 2-(1,3-benzothiazol-2-yl)phenol. *cis*-Position of the benzothiazole fragments of the metallated ligands $\{M(bt)_2\}$ with respect to the donor N and O atoms of the

Table 1. Bond lengths (*d*, Å) and bond angles (φ, deg) in complexes **I**, **II**, and **IV**

Bond, angle	**I**				**II**				**IV**
$M–C_{bt}$	1.996(5)		1.998(5)		2.002(5)		2.010(3)		1.999(6)
$M–N_{bt}$	2.041(5)		2.068(5)		2.041(3)		2.054(3)		2.021(4)
$M–N_{hbt}$	2.251(5)				2.221(3)				2.008(4)
$M–O_{hbt}$	2.155(4)				2.151(2)				2.100(3)
$C_{bt}MN_{bt}$	80.5(2)	95.2(2)	81.3(2)	91.5(2)	80.1(1)	96.1(1)	80.3(1)	92.3(1)	80.4(2)
$N_{bt}MO_{hbt}$	98.2(2)		85.4(2)		98.7(1)		84.4(1)		97.8(2)
$O_{hbt}MN_{hbt}$	85.1(2)				84.9(1)				83.6(2)
$N_{hbt}MC_{bt}$	100.2(2)		172.4(2)		100.4(1)		171.2(7)		98.1(2)
$C_{bt}MC_{bt}$	87.2(2)				88.4(1)				–
$N_{bt}MN_{hbt}$	82.2(2)		99.4(2)		88.0(1)		99.9(1)		178.5(2)
$C_{bt}MO_{hbt}$	87.5(2)		174.5(2)		86.4(1)		174.5(1)		173.2(2)
$N_{bt}MN_{bt}$	171.9(2)				171.8(1)				–

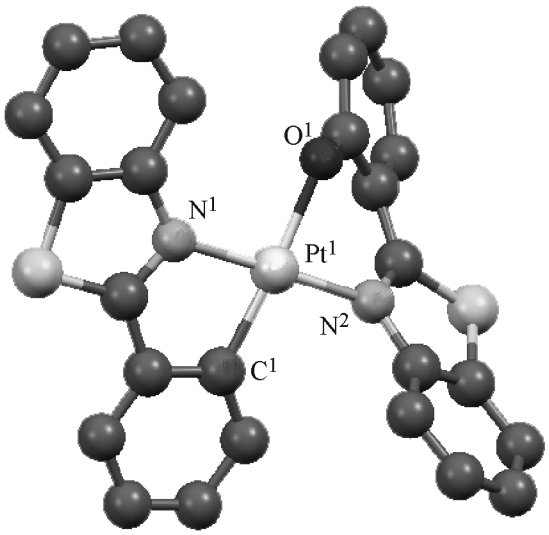

Fig. 2. Spatial structure of the [Pt(bt)hbt] complex in the crystal state (H atoms are omitted).

chelating ligand hbt^- resulted in the downfield and upfield shift of H^4 signal, respectively. Crystal lattice of [Pt(bt)hbt] contained a *trans*-N,N isomer (Fig. 2) typical of cyclometallated complexes of Pt(II) with chelating ligands [7]. The sum of bond angles of the donor atoms with Pt(II) of 359.9° corresponded to the planar position of platinum and the ligands donor atoms. The bond length between the metal and the C-metallated fragment {Pt(bt)} was practically the same in the cases of Rh(III), Ir(III), and Pt(II); the bond between the metal and N donor atom was shorter by 0.05–0.03 Å in the case of Pt(II) (Table 1). The difference in the bond length (by 0.24–0.21 Å and 0.06–0.05 Å) between the metal and the N and O donor atoms of the chelating ligand hbt^- in the cases of Pt(II) as compared to Rh(III) and Ir(III) complexes coincided with the enhanced *trans*-influence of C atom as compared to that of N atom of the platinated ligand {Pt(bt)}. In contrast to the platinated ligand with the benzothiazole and the phenyl fragments deviating from the coordination plane by no more than 2.6°, those fragments of the 2-(1,3-benzothiazol-2-yl)phenol chelating ligand deviated from the coordination plane by 24° and 31°, respectively.

Isomeric *trans*-N,N structure of [Pt(bt)hbt] in $CDCl_3$ solution was confirmed by NMR spectroscopy data. Despite the upfield shift of the C^4 signal of the platinated ligand {Pt(bt)}, the increase in its electronic density upon metalation resulted in a downfield shift of the H^4 signal by 1.50 ppm (Table 2). This pointed at anisotropic action of circular current of the phenyl ring in the *cis*-positioned ligand tilted by 31° with respect to the coordination plane; this fact confirmed the *trans*-N,N isomeric structure of the [Pt(bt)hbt] complex. The close chemical shifts and spin-spin coupling constants of the Pt(II) and Pd(II) complexes (Table 2) revealed the similar isomeric *trans*-N,N structure of the complexes.

Table 2. Coordination-induced changes of chemical shift ($\Delta = \delta_{complex} - \delta_{ligand}$, ppm) of the ligand atoms of **I**–**IV** in $CDCl_3$ solution

Comp. no.	NMR spectrum	Atom no.							
		4	5	6	7	3'	4'	5'	6'
		{M(bt)}							
I	^1H	0.8/–0.3	–0.4/–0.5	–0.5/–0.6	–0.3/–0.3	–1.0/–1.2	–0.3/–1.4	–0.6/–0.7	–0.7/–0.8
II	^1H	0.7/–0.3	–0.2/–0.2	–0.2/–0.2	–0.3/–0.3	–1.0/–1.2	–0.3/–1.3	–0.4/–0.5	–0.5/–0.9
III	^1H	1.5	0.1	0.0	–0.3	–0.4	0.0	–0.9	–0.5
IV	^1H	1.7	0.2	0.0	–0.3	–0.4	–0.1	–0.9	–0.6
	^{13}C	–1.2	1.6	0.5	0.0	7.9	1.3	0.19	–2.8
		{M(hbt)}							
I	^1H	–0.1	–0.4	–0.4	–0.5	–0.2	–0.7	0.0	–0.7
II	^1H	–0.1	–0.6	–0.6	–0.7	–0.2	–0.7	0.0	–0.7
III	^1H	0.2	0.0	0.0	–0.1	–0.5	–0.6	0.1	–0.4
IV	^1H	0.4	0.0	0.0	0.0	–0.4	–0.6	0.1	–0.2
	^{13}C	5.4	0.1	1.6	0.3	0.8	12.2	–13.3	4.9

Table 3. Optical and electrochemical properties of complexes **I**–**IV**

Complex	λ_{max}^{abs}, nm ($\varepsilon \times 10^3$ L mol^{-1} cm^{-1})	λ_{max}^{em}, nm	E_{eq}^{ox}, V[a]	E_{eq}^{red}, V[a]
I	268 (30.8), 316 (29.0), 410 (10.7), 440 sh (8.4)[b]	–	0.58	2.28
$[Rh(bt)_2En]^+$	266 (21.0), 280 sh (21), 318 (35.1), 400 (12.6)[c]	–	1.31	2.07
II	257 (42.7), 278 (40.6), 318 (33.8), 371 (12.7), 424 (10.1), 452 sh (9.5), 502 sh (5.0), 540 sh (2.3)[b]	566, 606 sh, 677 sh[b]	0.45	2.32
$[Ir(bt)_2En]^+$	261 (31.8), 294 (30.3), 312 (33.9), 324 (36.8), 379 sh (9.7), 430 (9.04), 460 sh (7.8)[c]	540, 569, 634 sh[c]	0.64	1.97
III	248 sh (30.7), 269 (26.2), 311 (21.4), 350 sh (10), 394 (7.02), 432 sh (6.0)[b]	–	0.60	2.17
$[Pd(bt)En]^+$	258 (14.5), 268 (10.7), 316 (14.9), 364 (10.7)[c]	–	1.30	2.31
IV	270 (33.7), 316 (23.4), 330 sh (20), 350 sh (10), 387 sh (7.4), 414 sh (9.7), 426 (10.1), 458 sh (5.8)[b]	540 sh, 578, 677 sh[b]	0.60	2.17
$[Pt(bt)En]^+$	260 (7.2), 302 sh (14.6), 314 (16.2), 327 (16.5), 399 (14.8)[c]	534, 576, 623 sh[c]	1.05	2.17

[a] $C_6H_5CH_3$–CH_3CN, 1 : 1. [b] 293 K, $CDCl_3$. [c] According to data [10].

The obtained results confirmed the *cis*-C,C and *trans*-N,N structure of the $[M(bt)_2hbt]$ [M = Rh(III) or Ir(III)] and [M(bt)hbt] [M = Pd(II) or Pt(II)] complexes in the crystalline form as well as in the solution, with the minor influence of the metal ion nature.

According to the model of localized molecular orbitals [8], the spin-allowed absorption bands and voltammograms of reduction and oxidation can be classified depending on the predominant localization of the molecular orbitals involved. Assuming the validity of the Koopmans' theorem [9], the similarity is anticipated between the nature of long-wave optical absorbance and the orbitals participating in the complexes reduction-oxidation.

Similarly to the $[M(bt)_2En]^+$ complexes with ethylenediamine chelating ligand [10], the absorption spectra of the $[M(bt)_2hbt]$ and [M(bt)hbt] complexes (Table 3) contained strong ($\varepsilon \sim 10^4$ L mol^{-1} cm^{-1}) intraligand π–π* optical transitions in the 250–330 nm region and weaker ($\varepsilon \sim 10^3$ L mol^{-1} cm^{-1}) bands assigned to the metal–ligand *d*–π* charge transfer, experiencing the red shift with the increasing energy of *d*-orbitals in the following series: Pd(II), Rh(III), Pt(II), Ir(III) (Fig. 3). The red shift of the absorption bands of metal–ligand charge transfer of the $[M(bt)_2hbt]$ and [M(bt)hbt] complexes by ~1900 cm^{-1} with respect to those of the complexes with ethylenediamine ligands reflected the increase in the metal d_π orbital energy due to π-donating properties of the hbt^- ligand. A special feature of absorption spectra of the $[M(bt)_2hbt]$ and [M(bt)hbt] complexes was the presence of the long-wave bands at 430–460 nm (Table 3), along with the bands of the above-discussed transitions. In the absorption spectrum of $[Ir(bt)_2hbt]$, both the spin-allowed optical transitions at 257–452 nm and the mixed singlet-triplet absorbance at 500–550 nm were observed, due to the enhanced spin-orbital interaction constant.

Voltammograms of the reduction of [M(bt)hbt] and $[M(bt)_2hbt]$ complexes showed an irreversible single-electron wave with the peak current potential of –(2.18±0.01) and –(2.30±0.02) V, being slightly ($\Delta E <$ 0.12 V) different from potential of reduction of the $[M(bt)En]^+$ and $[M(bt)_2En]^+$ complexes (Table 3). That allowed an assignment of the [M(bt)hbt] and $[M(bt)_2hbt]$ complexes reduction to the ligand-centered electron transfer to the LUMO predominantly localized at the π* orbitals of the {M(bt)} fragment.

$$[M(bt)hbt] + \bar{e} = [M(bt^-)hbt]^- \text{ [M = Pt(II), Pd(II)]},$$

$$[M(bt)_2hbt] + \bar{e} = [M(bt^-)(bt)hbt]^- \text{ [M = Ir(III), Rh(III)]}.$$

In contrast to the practically identical reduction potentials of the complexes with En and hbt^- chelating ligands, voltammograms of oxidation of the complexes were different (Fig. 4). The potential of the single-electron irreversible oxidation of the [M(bt)hbt] and

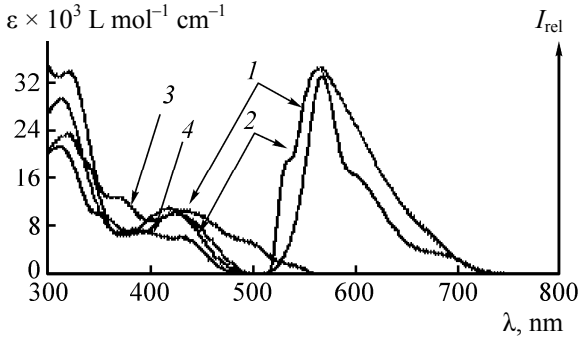

Fig. 3. Electron absorption and emission spectra of the (*1*) [Ir(bt)2hbt], (*2*) [Pt(bt)hbt], (*3*) [Rh(bt)2hbt], and (*4*) [Pd(bt)hbt] complexes solutions in CH_2Cl_2.

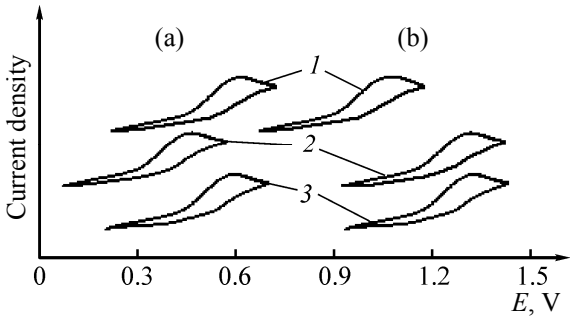

Fig. 4. Voltammograms of oxidation of the (a) [M(bt)hbt], [Rh(bt)2hbt] and (b) $[M(bt)En]^+$, $[Rh(bt)_2En]^+$ complexes. M = (*1*) Pt(II), (*2*) Pd(II), and (*3*) Rh(III).

$[M(bt)_2hbt]$ complexes (Table 3) was slightly dependent on the metal nature (0.52±0.08 V) and was shifted towards cathodic region as compared to the ethylenediamine complexes. The availability of the relatively high-energy occupied *p*-orbitals at the donor oxygen atom of the hbt^- ligand and the cathodic shift of the [Pt(bt)hbt], [Pd(bt)hbt], and $[Rh(bt)_2hbt]$ oxidation potential by more than 0.45 V allowed the assignment of their oxidation to the ligand-centered process.

$$[M(bt)hbt] - \bar{e} = [M(bt)(hbt)^+]^+ \; [M = Pt(II), Pd(II)],$$

$$[Rh(bt)_2hbt] - \bar{e} = [Rh(bt)_2(hbt^+)]^+.$$

The irreversible nature of the $[Ir(bt)_2hbt]$ complex oxidation coincided with the ligand-centered process operative as well. However, cathodic shift of the potential by 0.19 V with respect to the metal-centered oxidation of $[Ir(bt)_2En]^+$ could be due to the increase in the d_π orbitals energy resulting from π-donor properties of the hbt^- ligand. Therefore, the mixed d_π/p(O) HOMO could participate in the $[Ir(bt)_2hbt]$ oxidation.

Electrochemical experiments revealed that HOMO and LUMO of the [M(bt)hbt] [M = Pt(II), Pd(II)] and $[Rh(bt)_2hbt]$ complexes were predominantly localized at π*-orbitals of the bt^- metallated ligand and at *p* orbital of oxygen of the chelating ligand hbt^-. Assuming the validity of the Koopmans' theorem, the mentioned fact allowed the assignment of the long-wave absorbance bands at 430–460 nm to the optical ligand-ligand charge transfer, *p*(O)–π*(bt). LUMO of the $[Ir(bt)_2hbt]$ complex was mainly localized at the π*(bt) orbitals as well, whereas the HOMO was likely of the mixed d_π/p(O) nature, thus leading to the mixed nature of the spin-allowed long-wave absorbance band at 452 nm.

Photoexcitation (293 K) of solutions of the [Pt(bt)hbt] and $[Ir(bt)_2hbt]$ complexes in dichloromethane resulted in the complexes phosphorescence in the visible spectral range (Fig. 3). The slight red shift of the spectra as compared with those of the corresponding ethylenediamine complexes [10] by 210 and 850 cm^{-1} (Table 3) allowed assignment of the phosphorescence of [Pt(bt)hbt] and $[Ir(bt)_2hbt]$ complexes to the similar optical d_π–π*(bt) transition with the metal–ligand charge transfer. The absence of the phosphorescence in the cases of the Pd(II) and Rh(III) complexes in the solution was due to the typical thermal quenching resulting from the thermally induced population of the excited *d*–*d** states followed by fast chemical reaction [11].

To conclude, we demonstrated that HOMO and LUMO of the [M(bt)hbt] [M = Pt(II) or Pd(II)] and $[Rh(bt)_2hbt]$ complexes were predominantly located at the orbitals of the metallated and the chelating ligands, leading to the long-wave optical transition reflecting the ligand–ligand and ligand-centered reduction and oxidation of the complexes. LUMO of the $[Ir(bt)_2hbt]$ complex was mainly localized at the π* orbitals of the metallated ligand as well, but the complex HOMO was of the mixed d_π/p(O) nature due to the increased energy of the *d* orbitals of Ir(III). The latter fact resulted in the special features of the complex long-wave absorption and oxidation.

EXPERIMENTAL

One- and two-dimensional ^1H and ^{13}C NMR spectra of the solutions in $CDCl_3$ were recorded using a JNM-ECX400A spectrometer at the Center for Joint Usage, Department of Chemistry, Herzen Russian State

Table 4. Crystallographic parameters and structure refinement parameters of complexes **I**, **II**, and **IV**

Parameter	**I**	**II**	**IV**
Formula	$C_{39}H_{24}RhN_3OS_3$	$C_{39}H_{24}IrN_3OS_3$	$C_{26}H_{16}N_2OPtS_2$
Molar mass	749.70	838.99	631.62
Crystal system	Monoclinic	Monoclinic	Monoclinic
Space group	$P2_1/c$	$P2_1/c$	$P2_1/c$
a, Å	11.5036(2)	11.5207(7)	10.9485(4)
b, Å	15.0963(4)	15.0507(7)	13.7413(5)
c, Å	18.2650(5)	18.4118(10)	13.9391(5)
β	102.818(3)	102.859(6)	90.961(3)
V, Å^3	3092.89(13)	3095.5(3)	2096.8(1)
Z	4	4	4
d_{calc}, g/cm^3	1.610	1.800	2.001
μ, mm^{-1}	6.668	4.555	6.914
F(000)	1520.0	1648.0	1216.0
2θ, deg	5.24°–55°	5.16°–55°	5.56°–54°
Indexes	$-11 \le h \le 14$ $-9 \le k \le 18$ $-22 \le l \le 22$	$-11 \le h \le 14$ $-19 \le k \le 18$ $-23 \le l \le 23$	$-13 \le h \le 11$ $-17 \le k \le 16$ $-17 \le l \le 17$
Total reflections	6382	28653	10543
Independent reflections	5064	7006	4432
GoF	1.051	1.033	1.046
R factors [all data]	R_1 0.0720, wR_2 0.1805	R_1 0.0480, wR_2 0.0627	R_1 0.0462, wR_2 0.0805
ρ_{min}, ρ_{max}, e/Å^{-3}	1.000/0.374	1.39/–0.69	1.39/–0.69

$R_1 = \Sigma||F_0| - |F_c||/\Sigma|F_0|$; $wR_2 = \{\Sigma[w(F_0^2 - F_c^2)^2]/\Sigma[w(F_0^2)^2]\}^{1/2}$; $w = 1/[\sigma^2(F_0^2) + (aP)^2 + bP]$, with $P = (F_0^2 + 2F_c^2)/3$; $s = \{\Sigma[w(F_0^2 - F_c^2)]/(n-p)\}^{1/2}$, n = reflections number, p = number of refined parameters

Pedagogical University. Electron absorption and emission spectra of the solutions in CH_2Cl_2 were recorded using a SF-2000 spectrophotometer and a Flyuorat-2 Panorama spectrofluorimeter.

Voltammograms were obtained using an IPC-PRO device in the cell with the separated spaces of the working (glassy carbon), auxiliary (Pt), and reference (Ag) electrodes, using 0.1 mol/L solution of $[N(C_4H_9]PF_6$ in 1 : 1 $C_6H_5CH_3$–CH_3CN as background electrolyte. The peaks potentials were referenced to the ferrocenium/ferrocene redox system at 100 mV/s.

X-ray diffraction analysis was performed at 100 K using an Agilent Technologies Excalibur Eos diffractometer of the "X-ray diffraction methods" Resource Center, St. Petersburg State University (CCD detector, MoK_α radiation at λ 0.71073 Å). The crystallographic data and the structure refinement parameters of the [Rh(bt)$_2$hbt], [Ir(bt)$_2$hbt], and [Pt(bt)hbt] complexes are collected in Table 4. The unit cell parameters were refined using least-squares method. The structure was solved by the direct method and refined using SHELXL routine [12] implemented in OLEX2 software package [13] via the full-matrix least-squares method in the anisotropic approximation. The extinction was accounted for using the CrysAlisPro software [14]. Hydrogen atoms were introduced in the refinement with fixed positions and thermal parameters. The crystallographic data were deposited in the Cambridge Crystallographic Data Centre (CCDC 1006956, 996857, and 995845).

[Rh(bt)$_2$hbt], [Ir(bt)$_2$hbt], [Pd(bt)hbt], and [Pt(bt)hbt] complexes were prepared with yields of

about 50%, and the [Rh(bt)$_2$hbt] and [Ir(bt)$_2$hbt] complexes single crystals were prepared as described elsewhere [15].

[2-(1,3-Benzothiazol-2-yl)phenolato]bis[(2-phenyl-3-ido)-1,3-benzothiazole]rhodium(III) (I). ^{1}H NMR spectrum, δ, ppm (*J*, Hz): {Rh(bt)$_2$}, 8.89 m (H^4), 7.78 m (H^4), 7.70 d (H^{7,7}, $^3J_{HH}$ 7.9), 7.61 d (H$^{6'}$, $^3J_{HH}$ 7.5), 7.23 d (H$^{6'}$, $^3J_{HH}$ 7.9), 7.07 d.d (H$^{5,4'}$, $^3J_{HH}$ 8.5, 8.4), 7.05–6.91 m (H^{5,6}), 6.86 d.d (H^6, $^3J_{HH}$ 7.5, 7.4), 6.82 t.d (H$^{5'}$, $^3J_{HH}$ 6.9, $^4J_{HH}$ 1.6), 6.75 t.d (H$^{5'}$, $^3J_{HH}$ 7.6, $^4J_{HH}$ 0.8), 6.48 d (H$^{3'}$, $^3J_{HH}$ 8.4), 6.33 d (H$^{3'}$, $^3J_{HH}$ 7.7), 6.04 d.d (H$^{4'}$, $^3J_{HH}$ 7.6, 7.2); {Rh(hbt)}, 7.88 d (H^4, $^3J_{HH}$ 7.5), 7.28 m (H^7), 7.12 d.d (H^5, $^3J_{HH}$ 7.9, 7.4), 7.05–6.91 m (H$^{6,3'5'6'}$), 6.73 t (H$^{4'}$, $^3J_{HH}$ 7.4).

[2-(1,3-Benzothiazol-2-yl)phenolato]bis[(2-phenyl-3-ido)-1,3-benzothiazole]iridium(III) (II). ^{1}H NMR spectrum, δ, ppm (*J*, Hz): {Ir(bt)$_2$}, 8.82 d.d (H^4, $^3J_{HH}$ 9.1, $^4J_{HH}$ 1.9), 7.79 d.d (H^4, $^3J_{HH}$ 8.9, $^4J_{HH}$ 1.8), 7.70 d (H^7, $^3J_{HH}$ 7.1), 7.68 d (H^7, $^3J_{HH}$ 6.3), 7.59 d (H$^{6'}$, $^3J_{HH}$ 7.5), 7.32–7.24 m (H^{5,5,6,6}), 7.23 d (H$^{6'}$, $^3J_{HH}$ 7.3), 7.08 d.d (H$^{4'}$, $^3J_{HH}$ 8.3, 7.3), 6.98–6.91 m (H$^{5',5'}$), 6.48 d (H$^{3'}$, $^3J_{HH}$ 8.4), 6.23 d (H$^{3'}$, $^3J_{HH}$ 7.6), 6.09 d.d (H$^{4'}$, $^3J_{HH}$ 7.6, 7.1); {Ir(hbt)}, 7.90 d (H^4, $^3J_{HH}$ 7.6), 7.13 t.d (H^5, $^3J_{HH}$ 7.9, $^4J_{HH}$ 1.1), 6.98–6.91 m (H$^{7,6,5'}$), 6.71 d (H$^{3'}$, $^3J_{HH}$ 7.7), 6.59 d.d. d (H$^{4'}$, $^3J_{HH}$ 7.6, 7.2). ^{13}C NMR spectrum, δ_C, ppm: 180.0, 179.6, 169.6, 169.4, 151.4, 154.1, 151.0, 149.9, 149.1, 141.6, 141.3, 136.0, 132.9, 132.5, 131.3, 131.1, 130.7, 130.5, 130.4, 130.2, 128.0, 127.1, 126.6, 126.3, 125.5, 125.1, 124.8, 124.6, 123.2, 122.4, 122.2, 121.9, 121.8, 121.3, 120.4, 119.1, 114.4.

[2-(Benzothiazol-2-yl)phenolato][(2-phenyl-3-ido)-1,3-benzothiazol]palladium(II) (III). ^{1}H NMR spectrum, δ, ppm (*J*, Hz): {Pd(bt)}, 9.61 d (H^4, $^3J_{HH}$ 8.3), 7.83 d (H^7, $^3J_{HH}$ 7.0), 7.64 d.d (H^5, $^3J_{HH}$ 7.6, 7.8), 7.54 d (H$^{6'}$, $^3J_{HH}$ 7.5), 7.47 d.d (H^6, $^3J_{HH}$ 7.5. 7.3), 7.28 m (H$^{3'}$), 6.79 t (H$^{4'}$, $^3J_{HH}$ 7.4), 6.59 m (H$^{5'}$); {Pd(hbt)}, 8.20 m (H^4), 7.85 d (H^7, $^3J_{HH}$ 8.0), 7.45 t (H$^{5'}$, $^3J_{HH}$ 8.0), 7.38 m (H^{5,6}), 7.08 d (H$^{6'}$, $^3J_{HH}$ 8.4), 7.04 d.d (H$^{4'}$, $^3J_{HH}$ 7.5, 7.4), 6.59 m (H$^{3'}$).

[2-(Benzothiazol-2-yl)phenolato][(2-phenyl-3-ido)-1,3-benzothiazol]platinum(II) (IV). ^{1}H NMR spectrum, δ, ppm (*J*, Hz): {Pt(bt)}, 9.84 d (H^4, $^3J_{HH}$ 8.4), 7.82 m (H^7), 7.66 d.d (H^5, $^3J_{HH}$ 7.6, 7.5), 7.51 d.d (H$^{6'}$, $^3J_{HH}$ 7.6, $^4J_{HH}$ 1.4), 7.46 d.d (H^6, $^3J_{HH}$ 7.5, 7.3), 7.44 d (H$^{3'}$, $^3J_{HH}$ 7.6), 6.75 t.d (H$^{4'}$, $^3J_{HH}$ 7.5, $^4J_{HH}$ 0.9), 6.59 t (H$^{5'}$, $^3J_{HH}$ 7.3); {Pt(hbt)}, 8.34 m (H^4), 7.80 d (H^7, $^3J_{HH}$ 8.0), 7.40 m (H^{5,6}), 7.28 t.d (H$^{5'}$, $^3J_{HH}$ 7.5, $^4J_{HH}$ 1.5), 7.10 d (H$^{6'}$, $^3J_{HH}$ 8.4), 6.99 d.d (H$^{4'}$, $^3J_{HH}$ 7.7, 7.4), 6.70 d (H$^{3'}$, $^3J_{HH}$ 7.6). ^{13}C NMR spectrum, δ_C, ppm: {Pt(bt)}, 180.7 (C^1), 150.3 (C^3), 141.6 (C$^{1'}$), 136.3 (C$^{3'}$), 132.1 (C^8), 130.1 (C$^{4'}$), 127.6 (C^5), 125.5 (C^5), 124.8 (C$^{6'}$), 123.3 (C$^{5'}$), 121.8 (C$^{2',4}$), 121.4 (C^7); {Pt(hbt)}, 174.6 (C^1), 167.2 (C$^{2'}$), 150.7 (C^3), 134.7 (C$^{4'}$), 132.1 (C^8), 128.8 (C^{4,6}), 126.6 (C^5), 126.1 (C^4), 125.9 (C^6), 122.3 (C$^{3'}$), 121.8 (C^7), 121.4 (C$^{1'}$), 115.8 (C$^{5'}$).

ACKNOWLEDGMENTS

Authors express their gratitude to R.I. Baichurin and S.V. Makarenko (Center for Joint Usage, Department of Chemistry, Herzen Russian State Pedagogical University) for assistance with NMR spectra recording.

This work was financially supported by Ministry of Science and Education of the Russian Federation in the scope of governmental contract no. 4.131.2014K.

REFERENCES

1. Albrecht, M., *Chem. Rev*., 2010, vol. 110, no. 2, p. 576. DOI: 10.1021/cr900279a.
2. You, Y. and Nam, W., *Chem. Soc. Rev.,* 2012, vol. 41, no. 21, p. 7061. DOI: 10.1039/C2CS35171D.
3. Chi, Y. and Chou, P.T., *Chem. Soc. Rev*., 2010, vol. 39, no. 3, p. 638. DOI: 10.1039/B916237B.
4. Kubas, G.J., *J. Organometal. Chem*., 2009, vol. 694, no. 17, p. 2648. DOI: 10.1016/j.jorganchem.2009.05.027.
5. Leung, C.-H., Zhong, H.-J., Chan, D.S.-H., and Ma, D.-L., *Coord. Chem. Rev*., 2013, vol. 257, nos. 11–12, p. 1764. DOI: 10.1016/j.ccr.2013.01.034.
6. Zhao, Q., Li F. and Huang, C., *Chem. Soc. Rev*., 2010, vol. 39, no. 8, p. 3007. DOI: 10.1039/B915340C.
7. Liu, Y., Zhao, Q., Wu, H., Huang, K., and Li, F., *Inorg. Chem*., 2011, vol. 50, no. 13, p. 5969. DOI: 10.1021/ic102481x.
8. DeArmond, K., Hanck, K.W., and Wertz, D.W., *Coord. Chem. Rev*., 1985, vol. 64, p. 65. DOI: 10.1016/0010-8545(85)80042-4.
9. Koopmans, T., *Phisics.*, 1933, vol. 1, no. 1, p. 104.
10. Katlenok, E.A., Ivanova, E.V., Puzyk, M.V., and Balashev, K.P., *Optics Spectr*., 2012, vol. 113, no. 3, p. 279. DOI: 10.1134/S0030400X12090093.
11. Sajioto, A., Djurovich, P.A., Tamayo, A.B., Oxgaard, J., Goddard, W.A., and Thomson, M.E., *J. Am. Chem. Soc*., 2009, vol. 131, no. 28, p. 9813. DOI: 10.1021/ja903317w.
12. Sheldrick, G.M., *Acta Crystallogr. (A)*, 2008, vol. 64, no. 1, p. 112. DOI: 10.1107/S0108767307043930.
13. Dolomanov, O.V., Bourhis, L.J., Gildea, R.J., Howard, J.A.K., and Puschmann, H.*, J. Appl. Cryst.,* 2009, vol. 42, no. 2, p. 339. DOI: 10.1107/S0021889808042726.
14. *CrysAlisPro, Agilent Technologies*, Version 1.171.36.20, release 27-06-2012.
15. Liu, Y., Zhao, Q., Wu, H., Huang, K., and Li, F., *Inorg. Chem*., 2011, vol. 50, no. 13, p. 5969. DOI: 10.1021/ic102481x.